$^3[(d_{x^2-y^2}, d_{xy})(p_z)]$ Excited States of Binuclear Copper(I) Phosphine Complexes: Effect of Copper–Ligand and Copper–Copper Interactions on Excited State Properties and Photocatalytic Reductions of the 4,4′-Dimethyl-2,2′-bipyridinium Ion in Alcohols.

Zhong Mao, Hsiu-Yi Chao, Zheng Hui, Chi-Ming Che,* Wen-Fu Fu, Kung-Kai Cheung, and Nianyong Zhu[a]

Abstract: A comprehensive study of the structural and spectroscopic properties of two-, three-, and four-coordinate copper(I) complexes with aliphatic phosphine ligands is presented. All complexes described in this work are characterized by X-ray crystallography. The intramolecular Cu···Cu separations in $[Cu_2(dcpm)_2]X_2$, $[Cu_2(dcpm)_2(CH_3CN)_2]X_2$, and $[Cu_2(dmpm)_3](ClO_4)_2$ (dcpm = bis(dicyclohexylphosphino)methane; dmpm = bis(dimethylphosphino)methane; $X = ClO_4^-$ and PF_6^-) are in the range 2.639(2)–3.021(2) Å. The anion···Cu^I interaction is weak, as evidenced by the nearest O···Cu separation of 2.558(6) Å in $[Cu_2(dcpm)_2](ClO_4)_2$ and the closest Cu···F separation of 2.79(1) Å in $[Cu_2(dcpm)_2](PF_6)_2$. The absorption bands of $[Cu_2(dcpm)_2]X_2$ and $[Cu_2(dcpm)_2(CH_3CN)_2]X_2$ ($X = ClO_4^-$ and PF_6^-) at λ_{max} 307–311 nm in CH_2Cl_2 are assigned as $^1[3d\sigma^* \rightarrow 4p\sigma]$ transitions; this has been confirmed by resonance Raman spectroscopy. The triplet emissions in the visible region from these complexes exhibit long lifetimes and are sensitive to the environment. The lowest emissive excited state is tentatively ascribed as $^3[(d_{x^2-y^2}, d_{xy})(p_z)]$ in nature. For $[Cu_2(dcpm)_2]^{2+}$ salts in CH_3CN, the emissive species is postulated to be $[Cu_2(dcpm)_2(CH_3CN)_n]^{2+}$ ($n \geq 3$). Efficient photocatalytic reduction of MV^{2+} (4,4′-dimethyl-2,2′-bipyridinium) to MV^+ in alcoholic solutions by using $[Cu_2(dcpm)_2](PF_6)_2$ or $[Cu_2(dppm)_2(CH_3CN)_4](ClO_4)_2$ (dppm = bis(diphenylphosphino)methane) as a catalyst has been observed. The addition of CH_3CN or use of $[Cu_2(dmpm)_3](ClO_4)_2$ as a catalyst did not allow photocatalytic reduction processes to occur.

Keywords: copper · luminescence · metal–metal interactions · phosphanes · photochemistry

Introduction

Luminescent copper(I) complexes have generated considerable interest due to their rich photophysical properties[1] and potential applications in materials sciences.[2, 3] In the area of chemosensors, Ford and co-workers demonstrated significant changes in emission energy for $[\{CuI(4\text{-picoline})\}_4]$ when exposed to volatile organic solvents.[2] We recently reported the realization of organic light-emitting devices (OLEDs) derived from luminescent copper(I) arylacetylide complexes as light-emitting materials.[3] While the triplet metal-to-ligand charge-transfer (MLCT) emissions of copper(I) complexes containing aromatic diimine ligands is well documented in the literature,[1d, 4] there are a number of copper(I) complexes that contain ligands without low-energy π* orbitals, but display intense long-lived phosphorescence in the visible region under ambient conditions. Notable examples of these are the tri-, tetra-, and hexanuclear copper(I) complexes with chalcogenide capping ligands.[5] For photoluminescent polynuclear copper(I) complexes that display Cu···Cu contacts of less than 3.0 Å, Cu^I···Cu^I interactions are invariably invoked in the spectral assignment of their emissions.[1b,e, 2, 5, 6]

Recently, we communicated spectroscopic evidence for a metal—metal-bonded singlet $[d\sigma^*p\sigma]$ excited state in dinuclear copper(I) complexes.[7] The strong UV absorption of $[Cu_2(dcpm)_2]^{2+}$ salts with Cu···Cu distances of 2.639(2)–2.790(5) Å occurs at λ_{max} 307–311 nm and is assigned to the

[a] Prof. Dr. C.-M. Che, Z. Mao, Dr. H.-Y. Chao, Dr. Z. Hui, Dr. W.-F. Fu, Dr. K.-K. Cheung, Dr. N. Zhu
Department of Chemistry
and HKU-CAS Joint Laboratory on New Materials
The University of Hong Kong, Pokfulam Road
Hong Kong SAR (P.R. China)
Fax: (+852) 2857-1586
E-mail: cmche@hku.hk

Supporting information for this article is available on the WWW under http://www.chemeurj.org or from the author. Study of the reaction of $[Cu_2(dcpm)_2](PF_6)_2$ with CH_3CN, ^{31}P NMR chemical shift for **1** in CD_3CN and CD_2Cl_2 at various temperatures, perspective views of cations of **2, 5**, and **7**, and solid-state emission spectra of **6** and **7** at 298 K. Electronic absorption spectra of **9** in H_2O and CH_3CN, absorption, excitation, and emission spectra of **9** in aqueous solution at 298 K, UV-visible spectral changes of **2** and MV^{2+} in methanol as a function of irradiation time, and UV-visible spectral changes of $[Cu(dppm)_2(CH_3CN)_4](ClO_4)_2$ and MV^{2+} in ethanol as a function of irradiation time.

 DOI: 10.1002/chem.200204610

[3dσ* → 4pσ] transition. Based on resonance Raman experiments, it was suggested that the Cu – Cu interaction is stronger in the excited state than the ground state.[7] The emission of $[Cu_2(dcpm)_2]^{2+}$ was significantly affected by its micro-environment; it was virtually nonemissive in CH_2Cl_2 (quantum yield $< 10^{-4}$), but emitted at different energies from 77 K glass to 298 K CH_3CN solution. Furthermore, the proximity of counteranions to the copper(I) ions in the crystal lattices of $[Cu_2(dcpm)_2]X_2$ significantly affected the solid-state photoluminescent properties.[7]

The question arises as to the nature of the emissive excited state for dinuclear/polynuclear copper(I) complexes with and without $Cu^I \cdots Cu^I$ interactions. For three-coordinate d^{10}-gold phosphine complexes, we and Gray et al. have suggested that the $^3[(d_{x^2-y^2}, d_{xy})(p\sigma)]$ {or $^3[(d_{x^2-y^2}, d_{xy})(p_z)$}} for mononuclear gold(I)} excited state may be more important than $^3[d\sigma^*p\sigma]$ with respect to their influence on the photoluminescent characteristics.[8]

In this paper, an extensive study of the spectroscopic properties of two-, three-, and four-coordinate copper(I) complexes with aliphatic UV-silent phosphine ligands is described. Based on the findings in this work, we propose that the intermolecular copper···ligand interaction(s), both in the ground and excited states, is a key factor in determining the photophysical properties of di- and polynuclear copper(I) complexes. This also indicates that their lowest emissive electronic excited state is $^3[(d_{x^2-y^2}, d_{xy})(p_z)]$ in nature, and the long emission lifetime can be attributed to the forbidden nature of the $(d_{x^2-y^2}, d_{xy}) \rightarrow p_z$ transition. In addition, the efficient photocatalytic reduction of MV^{2+} (4,4′-dimethyl-2,2′-bipyridinium) to the MV^+ radical in alcoholic solutions by using $[Cu_2(dcpm)_2](PF_6)_2$ or $[Cu_2(dppm)_2(CH_3CN)_4](ClO_4)_2$ as a catalyst is described, and a reactive $[Cu_2(dcpm)_2]^{3+}$ intermediate capable of alcohol oxidation is postulated.

Results and Discussion

Synthesis: Two- and four-coordinate copper(I) phosphine complexes have been studied less than their three-coordinate analogues; the formation of the former requires sterically bulky auxiliary ligands such as tribenzyl-[9] or tricyclohexylphosphine. Recently, Hoffmann and co-workers reported dinuclear two-coordinate copper(I) complexes supported by the bulky bis(di-*tert*-butylphosphino)methane ligand.[10] We previously communicated the synthesis and spectroscopic properties of $[Cu_2(dcpm)_2]^{2+}$ salts.[7] Although $[Cu(PR_3)_2]^+$ and $[Cu(PR_3)X]_2$ derivatives were reported as early as 1970,[11] their photophysical properties have not been reported previously.

Here, $[Cu(CH_3CN)_4]X$ ($X = ClO_4^-$ and PF_6^-) were used as starting materials for the preparation of the mono- and dinuclear copper(I) phosphine complexes **1**, **2**, and **4**–**9** (Scheme 1). Reactions of $[Cu(CH_3CN)_4]X$ with dcpm in dry acetone or dichloromethane gave two kinds of products, depending on the dcpm/Cu molar ratio; a 1:1 ratio gave $[Cu_2(dcpm)_2]X_2$ ($X = ClO_4^-$ (**1**), PF_6^- (**2**)), whereas a 2:1 ratio gave $[Cu(dcpm)_2](PF_6)$ (**8**). Complexes **1** and **2** are stable in CH_2Cl_2 for more than 30 minutes in the absence of the free dcpm ligand. Diffusion of diethyl ether into solutions of **1** and **2** in acetonitrile gave $[Cu_2(dcpm)_2(CH_3CN)_2]X_2$ ($X = ClO_4^-$ (**4**), PF_6^- (**5**)), in which the CH_3CN molecule is coordinated to Cu^I. Attempts to obtain $[Cu_2(dcpm)_2L_2]^{2+}$ by the treatment of $[Cu_2(dcpm)_2](ClO_4)_2$ (**1**) with L (L = PPh_3 or pyridine) were unsuccessful. Complex **3** was prepared by the reaction of CuI with dcpm in a 1:1 molar ratio. Mononuclear complexes $[Cu(PCy_3)_2]X$ ($X = ClO_4^-$ (**6**), PF_6^- (**7**)) were synthesized by reacting $[Cu(CH_3CN)_4]X$ with excess PCy_3 in acetone or dichloromethane. Reaction of $[Cu(CH_3CN)_4](ClO_4)$ with the less bulky dmpm ligand gave **9** instead of $[Cu_2(dcpm)_2](ClO_4)_2$. Complexes **1**–**9** are stable in the solid state with respect to air and moisture.

Crystal structures: Complexes **1**–**9** have been characterized by X-ray crystal analysis. The cations of **1** (Figure 1) and **2** (Supporting Information) consist of two copper(I) ions bridged by two dcpm ligands, with Cu–P bond lengths in the range 2.199(2) – 2.229(2) Å. The anion···Cu^I interaction is weak, as signified by the nearest Cu···O and Cu···F interactions of 2.558(6) Å in **1** and 2.79(1) Å in **2.** The anion···copper interaction is presumably responsible for the deviation of the P-Cu-P angle from the expected linear geometry (i.e. 162.48(8) and 165.67(9)° in **1** and 170.0(2)° in **2**). The intramolecular Cu···Cu distances of 2.639(2) and 2.731(2) Å in **1** and 2.790(5) Å in **2** (Table 1) fall in the range in which weak $Cu^I \cdots Cu^I$ interactions become feasible. The cations in **4** and **5** are essentially isostructural and indepen-

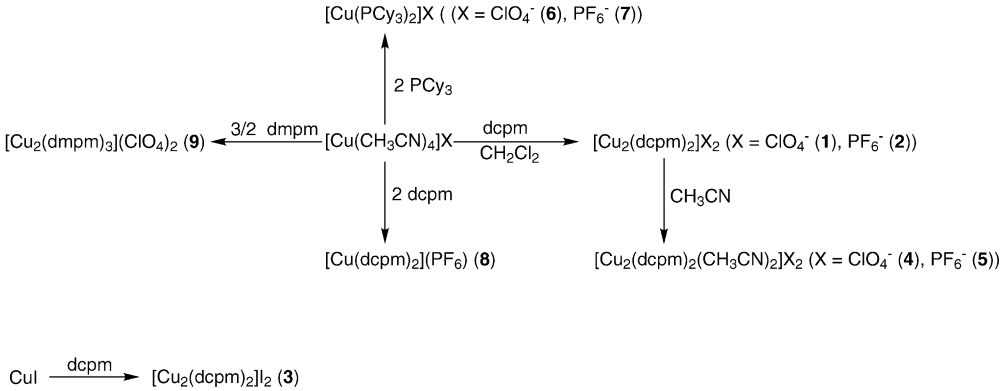

Scheme 1. Synthesis of **1**–**9**.

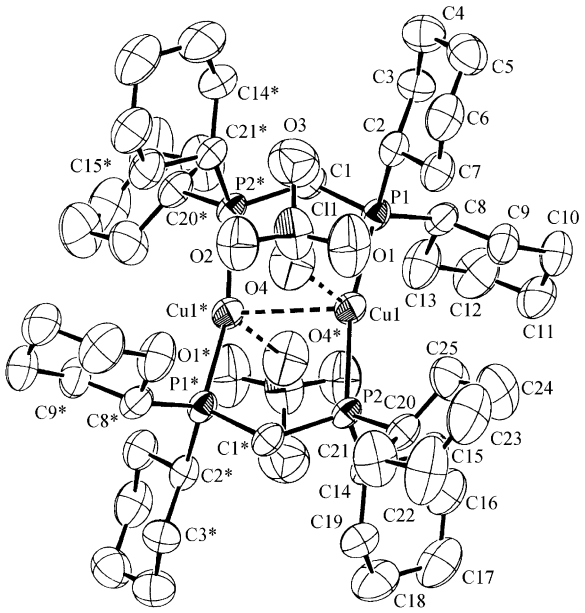

Figure 1. Perspective view of **1**. Selected bond lengths (Å) and angles (°) for one independent molecule: Cu1···Cu1* 2.731(2), Cu1···O 2.558(6), Cu1–P1 2.228(2), Cu1–P2 2.229(2), P1-Cu1-P2 162.48(8).

Table 1. Cu···Cu and shortest Cu···X distances, and P-Cu-P angles of complexes **1**–**7** and **9**.

Complexes	Cu···Cu [Å]	shortest Cu···X [Å]	P-Cu-P [°]
1	2.639(2), 2.731(2)	2.558(6) (X = O)	162.48(8), 165.67(9)
2	2.790(5)	2.79(1) (X = F)	170.0(2)
3	2.872(2), 2.938(2)		141.84(8), 145.24(7)
4	2.810(1)		143.86(4)
5	2.810(2)		146.1(1), 146.2(1)
6		2.26(1) (X = O)	144.44(9)
7		3.072(3) (X = F)	179.47(3)
9	3.021(2)	2.77(1) (X = O)	117.6(1), 118.4(1)
			120.1(1), 121.2(1)

dent of the counteranions. Figure 2 shows the $[Cu_2(dcpm)_2(CH_3CN)_2]^{2+}$ core in **4** (for **5**, see Supporting Information). The Cu^I atoms exhibit Y-shaped trigonal CuP_2N configurations. The P-Cu-P angles in **4** (143.86(4)°) and **5** (146.1(1) and 146.2(1)°) are considerably smaller than those in **1** and **2**, suggesting that the CH_3CN molecules engage in stronger interaction with the Cu^I core than the ClO_4^- and PF_6^- species. The Cu···Cu bond distances **4** and **5** are 2.810(1) and 2.810(2) Å, respectively, which are noticeably longer than those in **1** and **2**. Complex **3** features a three-coordinate copper(I) configuration (Figure 3). The Cu–I bond lengths are 2.621(1) and 2.623(1) Å, while the Cu–P bond lengths (2.248(2) and 2.254(2) Å), and P-Cu-P angles (141.84(8) and 145.24(7)°) are comparable to those in **4** and **5**. The intramolecular Cu···Cu separations in **3** are 2.872(2) and 2.938(2) Å; these are the longest among the dinuclear derivatives **1**–**5** (Table 1).

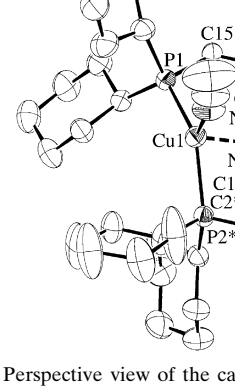

Figure 2. Perspective view of the cation of **4**. Selected bond lengths (Å) and angles (°): Cu1···Cu1* 2.8096(9), Cu1–N1 2.029(4), Cu1–P1 2.248(1), Cu1–P2* 2.249(1), P1-Cu1-P2* 143.86(4), P1-Cu1-N1 108.8(1), P2*-Cu1-N1 105.7(1).

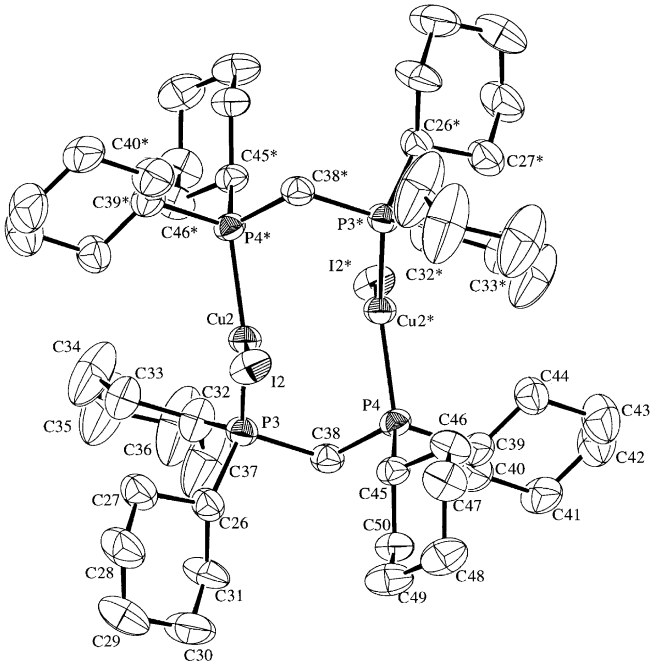

Figure 3. Perspective view of **3**. Selected bond lengths (Å) and angles (°): Cu2···Cu2* 2.872(2), Cu2–I2 2.621(1), Cu2–P3 2.248(2), Cu2–P4* 2.254(2), P3-Cu2-P4* 141.84(8), P3–Cu2–I2 114.27(6), P4*-Cu2-I2 103.08(5).

Complex **8** is four-coordinate with two chelating dcpm ligands. To the best of our knowledge, the structures of $[Cu(PR_2CH_2PR_2)_2]^+$ complexes have not been reported. As depicted in Figure 4, the Cu^I center adopts a distorted tetrahedral geometry with P-Cu-P angles of 75.74(3)–130.44(3)°. The Cu–P bond length (2.351(1) to 2.376(1) Å) is significantly longer than those in the dinuclear complexes **1**–**5** (2.199(2) to 2.254(2) Å). Figure 5 shows a perspective view of the cation in **9**. The $[Cu_2(dmpm)_3]^{2+}$ core adopts a 'manxane' structure[12] similar to $[Pt_2(dppm)_3]$[13] and $[Au_2(dmpm)_3]^{2+}$.[14] The P-Cu-P angles are 117.6(1)–121.2(1)°, which are normal for trigonal planar copper(I) complexes. The ClO_4^- ion is noncoordinating (nearest Cu···O distance 2.77(1) Å). The intramolecular Cu···Cu distance is 3.021(2) Å, which is noticeably longer than those in **1** and **2** (2.639(2)–2.790(5) Å). The Cu–P bond lengths range from 2.246(3) to 2.261(3) Å and are comparable to those observed in **3**–**5**.

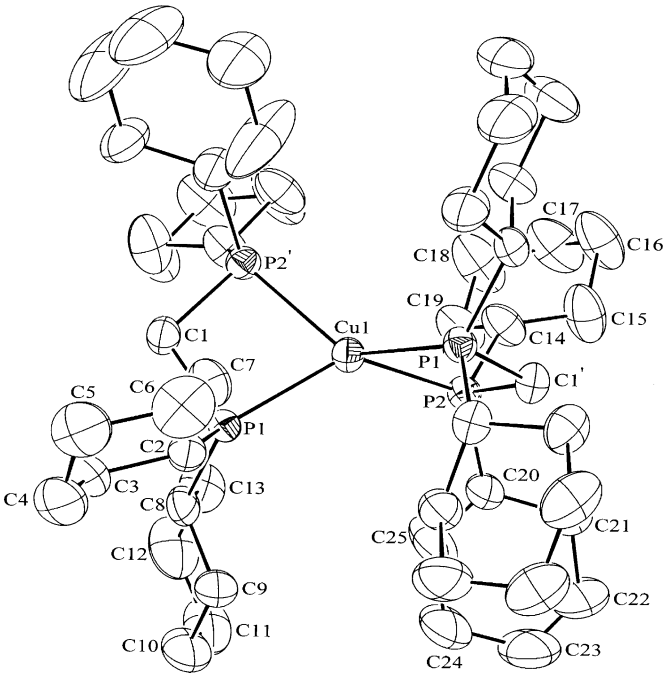

Figure 4. Perspective view of the cation of **8**. Selected bond lengths (Å) and angles (°): Cu1–P1 2.351(1), Cu1–P2 2.376(1), P1-Cu1-P2 130.43(3), P1-Cu1-P2′ 75.74(3), P1-Cu1-P1′ 122.98(5), P2-Cu1-P2′ 130.16(5).

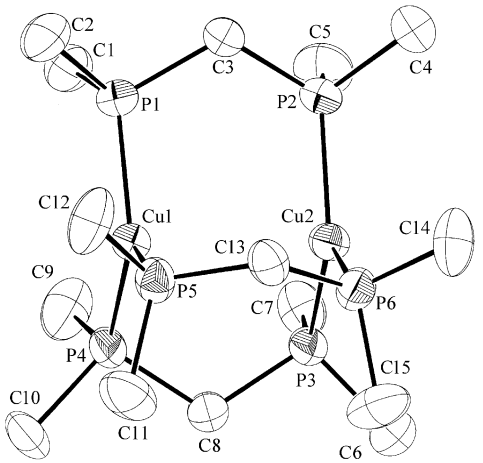

Figure 5. Perspective view of the cation of **9**. Selected bond lengths (Å) and angles (°): Cu1···Cu2 3.021(2), Cu1–P1 2.239(3), Cu1–P4 2.246(3), Cu1–P5 2.250(3), P1-Cu1-P4 121.2(1), P1-Cu1-P5 118.4(1), P4-Cu1-P5 120.1(1).

The structure of **6** was reported in 1975, [15] and we have obtained a similar structure in this work. The structure of the cation in **7** (Supporting Information) is similar to that of **6** except the $Cu^{I}\cdots$anion distances in the latter are sufficiently short for significant interaction. The closest Cu···O distance in **6** is 2.26(1) Å (comparable with 2.220(7) Å reported earlier[15]), which is longer than the sum of covalent radii (1.98 Å), but close to the sum of ionic radii (2.17 Å). The P-Cu-P angles in **6** and **7** are 144.44(9) and 179.47(3)°, respectively. Apparently, the $ClO_4^-\cdots[Cu(PCy_3)_2]^+$ interaction is stronger than that for $PF_6^-\cdots[Cu(PCy_3)_2]^+$.

Electronic absorption and ^{31}P NMR spectroscopy: The photophysical data of **1**–**9** are listed in Table 2. Complexes **1** and **4**, like **2** and **5**, display identical absorption spectra in CH_2Cl_2 except for minor differences in ε values. Figure 6 displays the electronic absorption spectra of **1** and **6** in CH_2Cl_2 and **1** in CH_3CN. An intense absorption band is observed at 311 nm for **1** ($\varepsilon \sim 1.4\times10^4$ dm^{3}mol^{-1}cm^{-1}) and at 307 nm for **2** ($\varepsilon \sim 1.7\times10^4$ dm^{3}mol^{-1}cm^{-1}) in CH_2Cl_2. Since the mononuclear complex **6** does not exhibit any significant absorption above 280 nm, we assign the intense absorptions for **1** and **2** to $^1[3d\sigma^* \rightarrow 4p\sigma]$ transitions. Previous results from resonance Raman measurements also supported this assignment.[7] The small difference in absorption maxima between **1** and **2** in CH_2Cl_2 may be attributed to the effect of the anion upon the $Cu^{I}\cdots Cu^{I}$ interaction in the ground state. As revealed by X-ray crystal analysis, the $[Cu_2(dcpm)_2]^{2+}$ core weakly interacts with counterions/solvent molecules in the crystal lattice of **1**, **2**, **4**, and **5**. The blue shift of the $3d\sigma^* \rightarrow 4p\sigma$ transition from **1** (311 nm) to **2** (307 nm) is consistent with the shorter Cu···Cu separation in **1** (mean 2.685 Å) relative to **2** (2.790(5) Å).

The electronic absorption spectrum of **9** in water shows an intense band at 276 nm. Since the intensity and shape of this band are similar to those for the $^1[3d\sigma^* \rightarrow 4p\sigma]$ transition of **1**, it is similarly assigned. The Cu···Cu distance in **9** (3.021(2) Å) is significantly longer than that in **1** (2.639(2) and 2.731(2) Å), and this may be correlated to the red shift of the metal-centered $^1[3d\sigma^* \rightarrow 4p\sigma]$ transition from 276 nm for **9** to 307 nm for **1**.

We found that the $^1[3d\sigma^* \rightarrow 4p\sigma]$ transition is affected by coordinating solvents. For the $[Cu_2(dcpm)_2]^{2+}$ species, the intense absorption band of **1**, **2**, **4**, and **5** at about 310 nm decreases in intensity and undergoes a red shift to about 319 nm when the fluid medium is changed from CH_2Cl_2 to CH_3CN. In a non-nitrile coordinating medium, such as CH_2Cl_2/MeOH (1:1),[16] **1** shows absorption bands at 286 and 308 nm with ε values below 10^4 mol^{-1}dm^{3}cm^{-1} (Table 2). For **9**, the intense absorption band at 276 nm in H_2O becomes featureless in CH_3CN and is replaced by a broad absorption at 240–300 nm (Supporting Information). Anion coordination at the Cu^{I} core also affects the $^1[3d\sigma^* \rightarrow 4p\sigma]$ transition. The absorption spectrum of complex **3**, which features a coordinated iodide moiety at each Cu^{I} center and a Cu···Cu separation of 2.872(2) and 2.938(2) Å, in CH_2Cl_2 shows a less prominent band at 323 nm ($\varepsilon \sim 3400$ mol^{-1}dm^{3}cm^{-1}), which is different from the intense 311 nm absorption band of **1** ($\varepsilon \sim 14\,100$ mol^{-1}dm^3 cm^{-1}). Other three-coordinate species such as $[\{Cu(PCy_3)Cl\}_2]$ and $[\{Cu(PCy_3)I\}_2]$, with two μ_2-halide groups, show intense absorption bands at 233 nm ($\varepsilon > 10^4$mol^{-1}dm^{3}cm^{-1}), while absorptions at $\lambda > 300$ nm exhibit very low εvalues (< 100mol^{-1}dm^{3}cm^{-1}) (Table 2).

It is pertinent to compare the absorption spectra of the dinuclear copper(I) phosphine derivatives **1**, **2**, **4**, and **5** with those of congeners bearing arylphosphine ligands, such as $[Cu_2(dppm)_2(CH_3CN)_4](ClO_4)_2$ and $[Cu_2(dppm)_2(L)_2](ClO_4)_2$ (L = PPh_3 or nitrogen bases).[17] The latter show broad absorption bands/shoulders at 306–315 nm ($\varepsilon = 8.54\times10^3$ to 4.19×10^4 mol^{-1}dm^{3}cm^{-1}) in CH_2Cl_2. Due to the low-lying $\pi\pi^*$ excited states of dppm and L, and the absence of $Cu^{I}\cdots Cu^{I}$

Table 2. Photophysical data of complexes **1**–**9**.

Complex	Medium (T [K])	λ_{abs} [nm] (ε [dm^{3}mol^{-1}cm^{-1}])	λ_{em} [nm]/τ[μs][a]	Φ_{em}
1[b]	CH_3CN (298)	269 (4830), 319 (4820)	480/4.2	0.048
	CH_2Cl_2 (298)[c]	278 (5840), 311 (14090)	~480 (w, br)	$<10^{-4}$
	CH_2Cl_2/MeOH (1:1) (298)	286 (6770), 308 (7310)	~600 (w, br)	$<10^{-4}$
	glass (77)[d]		420	
	solid (298)		475/44	
	solid (77)		384 (sh)/35, 476/120	
2	CH_3CN (298)	269 (4850), 319 (4830)	480/4.2	0.045
	CH_2Cl_2 (298)[c]	307 (16660)	~440 (w, br)	$<10^{-4}$
	glass (77)[d]		417/29	
	solid (298)		380/58, 475/63	
	solid (77)		379/30, 485/91	
3	CH_2Cl_2 (298)	280 (7410), 323 (3450)	485/2.4	5.7×10^{-4}
	glass (77)[d]		456/17	
	solid (298)		460/8.3	
	solid (77)		463/11	
4	CH_3CN (298)	269 (4880), 319 (4850)	480/4.4	0.046
	CH_2Cl_2 (298)[c]	278 (5590), 311 (13510)	~480 (w, br)	$<10^{-4}$
	glass (77)[d]		420/43	
	solid (298)		418/1.9	
	solid (77)		417/35	
5	CH_3CN (298)	269 (4890), 319 (4850)	480/4.4	0.044
	CH_2Cl_2 (298)[c]	307 (16550)	~440 (w, br)	$<10^{-4}$
	glass (77)[d]		420	
	solid (298)		411/8.2	
	solid (77)		411/42	
6	CH_3CN (298)	210 (23400), 230 (sh) (12500), 272 (900)	nonemissive	
	CH_2Cl_2 (298)[c]	239 (11500), 249 (9700), 275 (sh) (270)	nonemissive	
	glass (77)[d]		416/182[e]	
	solid (298)		491[e,f]	
	solid (77)		413/99[e]	
7	CH_3CN (298)	210 (22500), 230 (sh) (11500), 272 (880)	nonemissive	
	CH_2Cl_2 (298)	239 (11600), 249 (10300), 275 (sh) (120)	nonemissive	
	glass (77)[d]		416/183[e]	
	solid (298)		435/102[e]	
	solid (77)		412/108[e]	
8	CH_3CN (298)	253 (13800)	482	
	CH_2Cl_2 (298)	255 (28400)	nonemissive	
	glass (77)[d]		506	
	solid (298)		458/76	
	solid (77)		450/135	
9	H_2O (298)	276 (10800)	509/54	0.078
	CH_3CN (298)	264 (sh) (7380)	504/10.5	0.016
	glass (77)[d]		521	
	solid (298)		475/252	
	solid (77)		502	
$[Cu(PCy_3)Cl]_2$	CH_2Cl_2 (298)	233 (14000)	nonemissive	
	CH_3CN (298)	226 (18600)	nonemissive	
	solid (298)		430	
	solid (77)		428	
$[Cu(PCy_3)I]_2$	CH_2Cl_2 (298)	233 (26500), 285 (sh) (1240)	nonemissive	
	CH_3CN (298)	242 (23400), 287 (750)	nonemissive	
	solid (298)		454	
	solid (77)		454	

[a] For emission spectrum measurements, $\lambda_{ex}=330$ nm; for luminescence lifetime measurements, $\lambda_{ex}=355$nm. [b] In acetone, **1** shows very weak emission at 611 nm. In THF, decomposition occurred. [c] In dilute CH_2Cl_2 solution, slow decomposition occurred. [d] Solvent: EtOH/MeOH (1/4). [e] For emission spectrum measurements, $\lambda_{ex}=280$ nm; for luminescence lifetime measurements, $\lambda_{ex}=266$ nm. [f] Biexponential decay, τ_1: 3.2 μs; τ_2: 14.3 μs.

interactions (Cu···Cu separation > 3.7 Å) in these complexes, the 306–315 nm absorptions were assigned to metal-perturbed intraligand $\pi\rightarrow\pi^*$ transitions of dppm and L.

The ^{31}P NMR chemical shift of **1** (15.8 ppm) in CD_2Cl_2 is different from that of **2** (18.4 ppm), presumably due to the effect of anions upon the $[Cu_2(dcpm)_2]^{2+}$ core. Changing the temperature from 293 to 243 K resulted in minimal impact upon the ^{31}P NMR chemical shift of **1** (15.77 vs 15.43 ppm) in CD_2Cl_2 (Supporting Information). The ^{31}P NMR chemical shifts of **1**, **2**, **4**, and **5** in CD_3CN are virtually identical (9.8–9.9 ppm), and appear upfield from those recorded in CD_2Cl_2 (~15 ppm). It is noteworthy that the ^{31}P NMR chemical shift of **1** in CD_3CN is temperature-dependent and varies from 9.76 ppm at 293 K to 8.46 ppm at 243 K (Supporting Information). We tentatively attribute this to the rapid equilibrium process: $[Cu_2(dcpm)_2]^{2+} + n CH_3CN \rightleftharpoons$

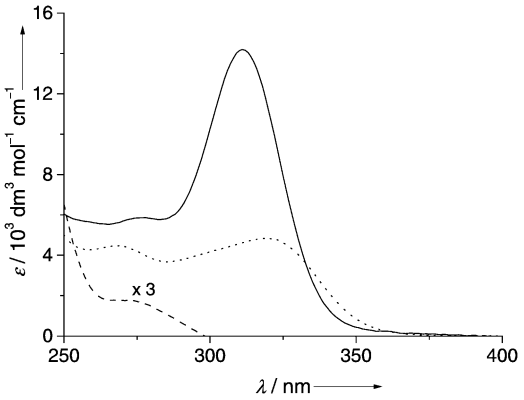

Figure 6. Electronic absorption spectra of **1** (solid line) and **6** (dashed line) in CH_2Cl_2, and **1** in CH_3CN (dotted line) at 298 K.

$[Cu_2(dcpm)_2(CH_3CN)_n]^{2+}$. Indeed, recrystallization of $[Cu_2(dcpm)_2]^{2+}$ in CH_3CN was found to give the $[Cu_2(dcpm)_2(CH_3CN)_2]^{2+}$ species, which was obtained as the ClO_4^- or PF_6^- salt. As discussed below, a minor population of $[Cu_2(dcpm)_2(CH_3CN)_n]^{2+}$ ($n \geq 3$) species is present in solutions of $[Cu_2(dcpm)_2]^{2+}$ salts in CH_3CN.

Solid-state emission spectroscopy: Here, the dinuclear copper(I)–dcpm complexes show intense photoluminescence in the solid state, and the emission energies are affected by the counterions and solvent molecules present in the respective crystal lattices (Table 2). Figure 7 shows the solid-state

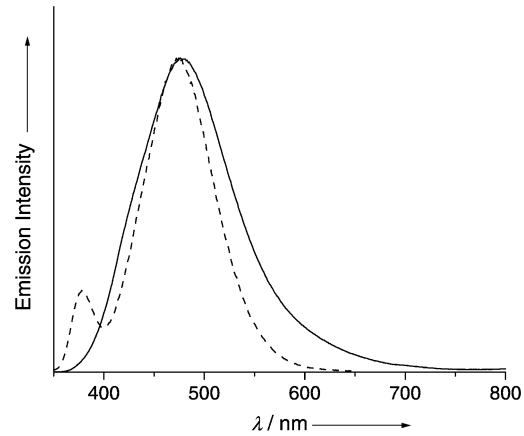

Figure 7. Solid-state emission spectra of **1** (solid line) and **2** (dashed line) at 298 K.

emission spectra of **1** and **2** at 298 K. Upon excitation at 280–350 nm, crystalline **1** emits at 475 nm with a lifetime of 44 μs. For **2**, a similar solid-state emission band at 475 nm (lifetime 63 μs) and a weak emission band at 380 nm (lifetime 58 ms) are observed. At 77 K, **1** displays solid-state emission at 384 (shoulder) and 476 nm. The solid-state emission maxima of **4** (418 nm) and **5** (411 nm) at 298 K are similar and higher in energy than those of **1** and **2** (~475 nm). In our previous study on related $[Au_2(dcpm)_2]X_2$ solids,[8e, 18] the high-energy emission at 360–370 nm was assigned to a $^3[5d\sigma^*6p\sigma]$ excited state, and the low-energy emission in the visible region was attributed to solvent/counteranion exciplex formation. We envision that the coordinative unsaturated copper(I) ions in $[Cu_2(dcpm)_2]^{2+}$ salts can also interact with solvent molecules/counterions in their vicinity, and such interactions are proposed to be responsible for the low-energy emission of **1** and **2** at $\lambda > 450$ nm. The weak high-energy solid-state emission observed at about 380 nm for **1** and **2** and at 411–418 nm for **4** and **5** may be tentatively assigned to the excited state directly populated by light excitation into the $3d\sigma^* \rightarrow 4p\sigma$ transition.

Upon excitation at 280 nm, the mononuclear complex **6** emits at 491 nm, while **7** emits at 435 nm in the solid state at 298 K (Supporting Information). With reference to the crystal data, the PF_6^- ion in **7** is distant from the Cu^I core, rendering copper–anion interactions unlikely. There is close contact between Cu^I and the ClO_4^- ion in **6**, and stabilization of the excited state by $Cu\cdots OClO_3^-$ interactions; this may account for the red shift in solid-state emission energy from **7** to **6**. At 77 K, the solid-state emission maxima of **6** and **7** are similar (~412 nm) and blue-shifted from that at 298 K. Complex **3**, a dinuclear complex with the Cu^I centers in trigonal planar geometry, emits at 460 nm (lifetime 8.3 μs) in the solid state at 298 K; lowering the temperature to 77 K does not affect the solid-state emission maximum. Similarly, the solid-state emission maxima of the dinuclear three-coordinate copper(I) complexes $[\{Cu(PCy_3)X\}_2]$ (X = Cl and I) are not influenced by decreasing the temperature from 298 to 77 K. Interestingly, $[\{Cu(PCy_3)Cl\}_2]$ exhibits a longer $Cu\cdots Cu$ separation than $[\{Cu(PCy_3)I\}_2]$ (3.07 vs 2.89 Å),[19, 20] yet the solid-state emission of the former appears at a higher energy (430 vs. 454 nm, respectively).

The solid-state emission spectrum of **8** at 298 K shows a broad and asymmetric band with λ_{max} at 458 nm. Upon lowering the temperature to 77 K, the bandwidth becomes narrow and a slight blue shift (λ_{max} 450 nm) is detected. This emission has a very long lifetime of 76 μs at 298 K and 135 μs at 77 K. A long-lived solid-state emission has also been observed for **9**. At 298 K, the emission maximum occurs at 475 nm with a lifetime of 252 μs, and this red-shifts to 502 nm at 77 K. The very long emission lifetime is indicative of the strongly forbidden nature of the transition responsible for radiative decay of the excited state.

Emission spectroscopy in fluid solutions: Complexes **1**, **2**, **4**, and **5** emit very weakly in CH_2Cl_2 (quantum yield $< 10^{-4}$), but emission at ~480 nm is "switched on" upon addition of CH_3CN. Addition of MeOH to a solution of **1** in CH_2Cl_2, however, did not give rise to a similar emission. Figure 8 shows the increase in emission intensity upon addition of CH_3CN to a solution of **2** in CH_2Cl_2. A nonlinear plot of emission intensity at 480 nm versus CH_3CN concentration was found, as depicted in the inset of Figure 8 (the concentration of **2** was kept at 2.4×10^{-4} mol dm^{-3}). Enhancement of the emission intensity at 480 nm is not prominent at CH_3CN concentrations below 1 mol dm^{-3}. However, at $[CH_3CN] \geq 10$ mol dm^{-3}, the 480 nm emission intensity increases sharply and continues even when $[CH_3CN]$ tends towards pure CH_3CN. The greatest intensity at 480 nm was found for **2** in pure CH_3CN. We have observed that CH_2Cl_2 only exerts a small quenching effect upon the

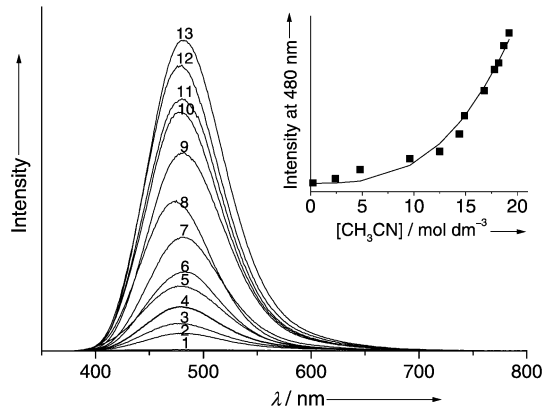

Figure 8. Emission spectral changes of **2** (2.4×10^{-4} M) in CH_2Cl_2 upon addition of CH_3CN ($\lambda_{ex}=310$ nm) at 298 K. Concentration of CH_3CN: 1) 0.05 M 2) 0.24 M 3) 2.4 M 4) 4.8 M 5) 9.6 M 6) 12.5 M 7) 14.4 M 8) 14.9 M 9) 16.6 M, 10) 17.8 M 11) 18.2 M 12) 18.7 M, 13) 19.2 M. Inset: Emission intensity at 480 nm vs. [CH_3CN] and theoretical fitting curve.

480 nm emission in CH_3CN (quenching rate constant $=6.9\times10^5$ $dm^3\,mol^{-1}\,s^{-1}$).

The experimental data was fitted to the equilibria, which is shown in Scheme 2. Details of these fittings are given in the Supporting Information. The data are not consistent

$$\text{Overall}\quad [Cu_2(dcpm)_2]^{2+} + n\,CH_3CN \overset{K}{\rightleftharpoons} [Cu_2(dcpm)_2(CH_3CN)_n]^{2+}$$

$$[Cu_2(dcpm)_2]^{2+} + CH_3CN \overset{K_{11}}{\rightleftharpoons} [Cu_2(dcpm)_2(CH_3CN)]^{2+}$$
$$[Cu_2(dcpm)_2(CH_3CN)]^{2+} + CH_3CN \overset{K_{12}}{\rightleftharpoons} [Cu_2(dcpm)_2(CH_3CN)_2]^{2+}$$
$$\vdots \qquad\qquad \vdots$$
$$[Cu_2(dcpm)_2(CH_3CN)_{n-1}]^{2+} + CH_3CN \overset{K_{1n}}{\rightleftharpoons} [Cu_2(dcpm)_2(CH_3CN)_n]^{2+}$$

Scheme 2. Experimental data fitted to the equilibria.

with the fitting for $n=1$ or 2, but match the fitting curve for $n=3$.[21] Thus, at sufficient [CH_3CN], the reaction shown in Equation 1 is proposed.:

$$[Cu_2(dcpm)_2]^{2+} + nCH_3CN \overset{K}{\rightleftharpoons} [Cu_2(dcpm)_2(CH_3CN)_n]^{2+} (n\geq 3) \qquad (1)$$

With $n=3$ and Equation S6 (Supporting Information), the fitting curve is shown in the inset of Figure 8. Even at a very high CH_3CN concentration (19.2 mol dm^{-3}), less than 1% of $[Cu_2(dcpm)_2]^{2+}$ undergoes reaction with CH_3CN molecules to give $[Cu_2(dcpm)_2(CH_3CN)_n]^{2+}$ species ($n\geq3$). Assuming $n=3$, the K, K_{11}, K_{12}, and K_{13} values were estimated to be 8×10^{-7} M^{-3}, 8×10^{-10}, 1, and 1×10^3 M^{-1}, respectively (Supporting Information). The low K value may explain the apparent lack of saturation for the emission intensity even when [CH_3CN] is nearly pure CH_3CN. Coordination of two CH_3CN molecules to a single Cu^I site in $[Cu_2(dcpm)_2]^{2+}$ would disrupt the weak $Cu^I\cdots Cu^I$ interaction, since the Cu^I center becomes tetrahedral. We noted that the related $[Cu_2(dppm)_2(CH_3CN)_4]^{2+}$ species contains a $Cu\cdots Cu$ separation of 3.757(3) Å.[22] Therefore, the 480 nm emission for CH_3CN solutions of $[Cu_2(dcpm)_2]^{2+}$ salts is tentatively assigned to the $^3[(d_{x^2-y^2}, d_{xy})(p_z)]$ excited state of the copper(I) core in $[Cu_2(dcpm)_2(CH_3CN)_n]^{2+}$ ($n\geq3$).

Similarly, interaction between CH_3CN and **9** is evident. The intense absorption band of **9** at 276 nm measured in aqueous solution is not present in acetonitrile (Supporting Information), but the emission recorded in these two solvents are similar in energy (CH_3CN: 504 nm; H_2O: 509 nm). The emission has a very long lifetime (54 μs) in aqueous solution. The absorption, excitation, and emission spectra of **9** measured in H_2O are shown in the Supporting Information, and the absorption and excitation spectra show a clear resemblance. We note that the Stokes shift between the $^1[3d\sigma^* \rightarrow 4p\sigma]$ absorption at 276 nm and the 509 nm emission band is 16600 cm^{-1}; this exceeds the expected singlet-triplet splitting of the $[d\sigma^*p\sigma]$ excited state. In the study of the Au^I analogue $[Au_2(dmpm)_3]^{2+}$, there is also a large Stokes shift of 22500 cm^{-1} between the $^3[(d_{x^2-y^2}, d_{xy})(p\sigma)]$ emission (604 nm) and the $^1[5d\sigma^* \rightarrow 6p\sigma]$ absorption bands (256 nm).[23] Thus, the emission of **9** at 509 nm is unlikely to originate directly from the 276 nm $^1[3d\sigma^* \rightarrow 4p\sigma]$ absorption. Since interaction between the two Cu^I atoms in **9** is extremely weak ($Cu\cdots Cu$ separation 3.021(2) Å) in the solid state, the d_{z^2} splitting cannot give a $d\sigma^*$ orbital that is higher in energy than ($d_{x^2-y^2}$, d_{xy}). We tentatively assign the emission of **9** to the $^3[(d_{x^2-y^2}, d_{xy})(p_z)]$ excited state. Previously,[17] the $[Cu_2(dppm)_2L_2]^{2+}$ (L = PPh_3 or nitrogen bases) complexes with three-coordinate copper(I) ions were found to emit strongly at 515–550 nm with long lifetimes (>24 μs) in CH_2Cl_2. As revealed by X-ray crystallography, there is no $Cu\cdots Cu$ interaction in these complexes (>3.7 Å) and, hence, low-energy $^1[3d\sigma^* \rightarrow 4p\sigma]$ transitions are not observed. Interestingly, the emission bands observed for $[Cu_2(dppm)_2L_2]^{2+}$, $[Cu_2(dcpm)_2(CH_3CN)_n]^{2+}$, and **9** occur at comparable energies irrespective of the presence or extent of $Cu\cdots Cu$ interaction among these complexes. These results are consistent with the assignment that the emission from all three derivatives originates from the $^3[(d_{x^2-y^2}, d_{xy})(p_z)]$ excited state of a copper(I) site with a coordination number of no less than three.

Photochemical reactions and photocatalysis: Previously,[24] we showed that $[Cu_2(dppm)_2(CH_3CN)_4]^{2+}$ can catalyze the light-induced carbon–carbon coupling reactions of alkyl halides. Here, we have found that the triplet excited states of binuclear copper(I) complexes with dcpm, dppm, and dmpm ligands are powerful reductants. Because of its extended excited-state lifetime and higher stability in solution, **9** was chosen as a prototypical example for evaluation of its excited-state redox properties.

The emission of **9** was quenched by pyridinium acceptors through an electron transfer mechanism. Figure 9 shows the transient absorption difference spectrum of a solution of **9** and MV^{2+} in CH_3CN recorded 1 μs after laser flashing at 355 nm. The two absorption maxima at 385 and 605 nm are assigned to $MV^{+\cdot}$, and the absorbance for both followed second-order decay kinetics (rate constant $=6.9\times10^7$ $dm^3\,mol^{-1}\,s^{-1}$) back to the original baseline. The proposed photochemical reaction is shown in Scheme 3. There is no net formation of $MV^{+\cdot}$ upon

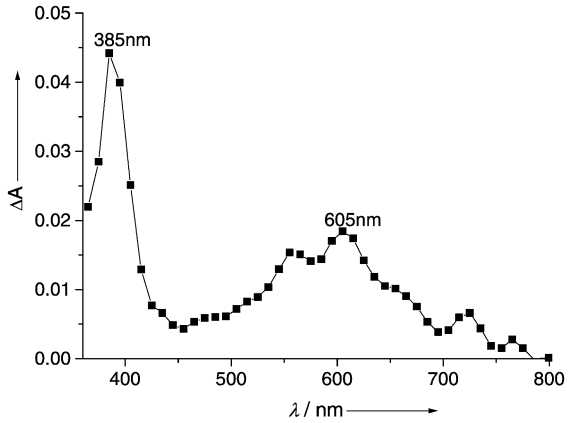

Figure 9. Transient absorption difference spectrum recorded 1 μs after laser flashing for a solution of **9** (2.21×10^{-4} M) and MV^{2+} (1.12×10^{-2} M) in CH_3CN.

$$[Cu_2(dmpm)_3]^{2+*} + MV^{2+} \longrightarrow [Cu_2(dmpm)_3]^{3+} + MV^{\cdot+}$$

$$[Cu_2(dmpm)_3]^{3+} \longrightarrow [Cu_2(dmpm)_3]^{2+} + MV^{2+}$$

Scheme 3. Proposed photochemical reaction.

photolysis of a solution of **9** and MV^{2+} in methanol with a 100 W Xenon lamp for one hour. Other pyridinium acceptors also quenched the emission of $[Cu_2(dmpm)_3]^{2+*}$ at 509 nm. The quenching rate constants were determined by Stern–Volmer kinetics experiments and the data are listed in Table 3. Upon fitting the rate constants by using the Rehm-Weller equation, the excited-state redox potential ($E^{\circ}[Cu_2(dmpm)_3{}^{3+/2+*}]$) and the reorganization energy (λ) are determined to be -1.55 V vs SSCE (sodium chloride saturated calomel electrode) and 0.76 eV, respectively.

Table 3. Rate constants for the electron-transfer reaction between **9** and pyridinium ions in methanol at 298 K.

Pyridinium ions (Q)[a]	$E^{\circ}(Q^{+}/Q)$ (vs SSCE)[b]	k_q [$dm^3 mol^{-1} s^{-1}$]	k_q'[c] [$dm^3 mol^{-1} s^{-1}$]	$\ln k_q'$
4-cyano-*N*-methylpyridinium	−0.67	1.94×10^9	2.41×10^9	21.60
4-methylcarbonyl-*N*-methylpyridinium	−0.78	1.13×10^9	1.27×10^9	20.96
4-amido-*N*-ethylpyridinium	−0.93	7.32×10^8	7.90×10^8	20.49
3-amido-*N*-benzylpyridinium	−1.07	5.90×10^8	6.27×10^8	20.26
3-amido-*N*-methylpyridinium	−1.14	4.18×10^8	4.36×10^8	19.89
N-ethylpyridinium	−1.36	1.08×10^8	1.09×10^8	18.51
4-methyl-*N*-methylpyridinium	−1.49	1.41×10^7	1.41×10^7	16.46

[a] All of the compounds are either hexafluorophosphate or trifluoromethanesulphonate salts. [b] J. L. Marshall, S. R. Stobart, H. B. Gray, *J. Am. Chem. Soc.* **1984**, *106*, 3027–3029. [c] $(1/k_q') = (1/k_q) - (1/k_d)$, in which k_d is the

The emission of **9** was also quenched by *N*,*N*,*N*′,*N*′-tetramethylphenylenediamine (TMPD) with a rate constant of 6.9×10^9 $dm^3 mol^{-1} s^{-1}$. The transient absorption difference spectrum for a solution of **9** in CH_3CN, in the presence of TMPD recorded 5 μs after laser flashing, shows the absorption peak maxima at 560 and 610 nm attributable to $TMPD^{\cdot+}$. The photochemistry of $[Cu_2(dmpm)_3]^{2+}$ in aqueous solution has also been studied; the emission of $[Cu_2(dmpm)_3]^{2+*}$ was quenched by using formic acid at a rate constant of 1.5×10^4 $dm^3 mol^{-1} s^{-1}$.

The emissions of $[Cu_2(dcpm)_2]^{2+}$ salts were also quenched by pyridinium acceptors. However, unlike **9**, facile net photoredox reactions were readily observed upon laser-flash photolysis of a solution of **2** and MV^{2+} in CH_3CN at 355 nm excitation, and the reaction became very facile in ethanol or methanol. Figure 10 shows the UV-visible spectral changes of **2** (9.71×10^{-6} M) and MV^{2+} (2.04×10^{-4} M) in ethanol upon excitation with a 100 W Xenon lamp (using a filter with cut-off wavelength at 295 nm) at different time intervals (the UV-visible spectral changes of **2** and MV^{2+} in methanol are shown in the Supporting Information). The $MV^{\cdot+}$ species was readily generated and characterized by its absorption maxima at 396 and 607 nm. This signal remained stable and did not decay for several hours. The absorbance at 607 nm attributed to $MV^{\cdot+}$ reached a maximum after irradiation for 35 minutes (the inset of Figure 10), while the absorbance of MV^{2+} at λ_{max} 260 nm decreased with irradiation. We found that at a fixed concentration of MV^{2+} (2.04×10^{-4} M), increasing the concentration of **2** resulted in rapid growth of the absorbance at 607 nm. Based on the absorbance at 607 nm ($\varepsilon = 1.37 \times 10^4$ $dm^3 mol^{-1} cm^{-1}$),[25] the $MV^{\cdot+}$ concentration can be derived. We found that one molar equivalent of **2** generated more than five equivalents of $MV^{\cdot+}$ in methanol and more than ten equivalents of $MV^{\cdot+}$ in ethanol; hence, net photocatalytic reductions of MV^{2+} have been demonstrated.

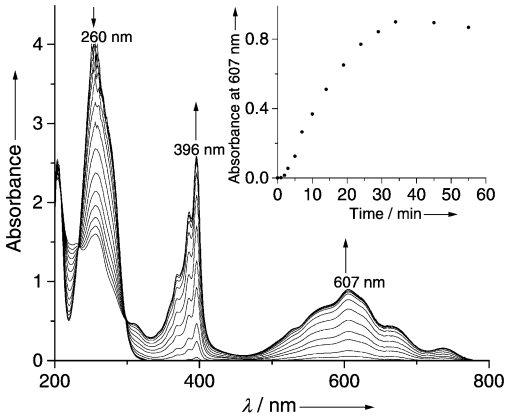

Figure 10. UV-visible spectral changes of **2** (9.71×10^{-6} M) and MV^{2+} (2.04×10^{-4} M) in ethanol as a function of irradiation time. Inset: Absorbance at 607 nm as a function of irradiation time.

We suggest that the photochemically generated $[Cu^{I}Cu^{II}(dcpm)_2]^{3+}$ species is highly reactive and rapidly reacts with alcohol to regenerate the $[Cu_2(dcpm)_2]^{2+}$ precursor [Eqs. (2) and (3)]. Attempts to determine the oxidized

$$[Cu_2(dcpm)_2]^{2+*} + MV^{2+} \longrightarrow [Cu^{I}Cu^{II}(dcpm)_2]^{3+} + MV^{+} \quad (2)$$

$$[Cu^{I}Cu^{II}(dcpm)_2]^{3+} + \text{alcohol} \longrightarrow [Cu_2(dcpm)_2]^{2+} + \text{oxidized product} \quad (3)$$

organic products were not successful, presumably due to the very low concentrations present.

We have also performed laser-flash photolysis of a solution of $[Cu_2(dppm)_2(CH_3CN)_4](ClO_4)_2$ and MV^{2+} in ethanol; this revealed a similar net photochemical reaction. The UV-visible spectral changes of $[Cu_2(dppm)_2(CH_3CN)_4](ClO_4)_2$ (7.79×10^{-6} M) and MV^{2+} (1.99×10^{-4} M) in ethanol are shown in the Supporting Information. The absorption band at 607 nm for $MV^{\cdot+}$ reached a maximum value after irradiation for 40 minutes, and we found that one molar equivalent of $[Cu_2(dppm)_2(CH_3CN)_4](ClO_4)_2$ produced more than ten equivalents of $MV^{\cdot+}$ in ethanol.

General Remarks: It is important to highlight the remarkable photoluminescent and photochemical characteristics of the copper(I) phosphine complexes described in this study. All the intriguing features can be attributed to the presence of reactive two-coordinate Cu sites.

The absence of emission for $[Cu_2(dcpm)_2]^{2+}$ in dichloromethane plus the similarities in emission energies for solutions of $[Cu_2(dcpm)_2]^{2+}$ and $[Cu_2(dmpm)_3]^{2+}$ in acetonitrile suggest that two-coordinate copper(I) species are not responsible for the visible photoluminescence at 480–504 nm. The unreasonably large Stokes shift between the $^1[3d\sigma^* \rightarrow 4p\sigma]$ transition at 307–320 nm and the visible emission bands of $[Cu_2(dcpm)_2]^{2+}$ salts at $\lambda > 450$ nm, together with the fitting of the emission intensity at 480 nm versus $[CH_3CN]$ (inset of Figure 8), indicate that the visible emissions of $[Cu_2(dcpm)_2]^{2+}$ solids and $[Cu_2(dcpm)_2]X_2$ species in CH_3CN do not originate from $^3[3d\sigma^*4p\sigma]$ excited states. The fitting results suggest that the emitting species in solutions of $[Cu_2(dcpm)_2]^{2+}$ in CH_3CN is $[Cu_2(dcpm)_2(CH_3CN)_n]^{2+}$ ($n \geq 3$). The $[3d\delta^* (d_{x^2-y^2}, d_{xy}) \rightarrow 4p\sigma]$ transition should exhibit a low oscillator strength due to poor overlap between $3d\delta^*$ and $4p\sigma$ orbitals. Thus the $^3[3d\delta^*(d_{x^2-y^2}, d_{xy})(4p\sigma)]$ excited state could have a long lifetime due to the strongly forbidden nature of the transition, and this can account for the long-lived visible emission from these copper(I) complexes. It should be emphasized that the observed emission lifetime for an aqueous solution of $[Cu_2(dmpm)_3]^{2+}$ (54 μs) is unusually long for metal-centered excited states of inorganic and organometallic complexes.

The open coordination sites of the $[Cu_2(dcpm)_2]^{2+}$ moiety accounts for its intriguing photoluminescent properties, which are sensitive to the close proximity of solvent/anion. This underscores the tremendous potential of two-coordinate copper(I) complexes in applications like molecular light switches by manipulating substrate binding reactions at Cu^I sites. The vacant coordination site is also responsible for the intriguing reactivity of the two-coordinate $[Cu_2(dcpm)_2]^{3+}$ species, generated in situ, in photo-induced oxidative quenching processes. Observation of catalytic reduction of MV^{2+} to $MV^{\cdot+}$ upon irradiation of alcoholic solutions of $[Cu_2(dcpm)_2]^{2+}$ and MV^{2+} suggests that the photogenerated $[Cu^ICu^{II}(dcpm)_2]^{3+}$ is very reactive and is readily reduced back to $[Cu^ICu^I(dcpm)_2]^{2+}$, presumably by oxidation of alcohol. Since the photochemical reaction was quenched in the presence of CH_3CN and not observed when $[Cu_2(dmpm)_3]^{2+}$ was used, a two-coordinate copper(II) moiety supported by electron-rich phosphine ligands is deemed to be the key structural motif for the observed photocatalytic reduction processes.

Experimental Section

Materials: Bis(dicyclohexylphosphino)methane (dcpm), bis(dimethylphosphino)methane (dmpm), and tricyclohexylphosphine (PCy_3) were purchased from Strem and used as received. $[Cu(CH_3CN)_4]X$ ($X = ClO_4^-$ and PF_6^-),[26] $[\{Cu(PCy_3)Cl\}_2]$,[19] and $[\{Cu(PCy_3)I\}_2]$[20] were prepared by the literature methods. All solvents for synthesis were of analytical grade and used as received, except acetone, which was distilled from P_2O_5. All reactions were performed under an inert atmosphere unless otherwise mentioned. Details of solvent purification for photophysical studies have been described elsewhere.[27] Syntheses of **1**–**6** have been communicated.[7]

$[Cu(PCy_3)_2]PF_6$ (7): A mixture of $[Cu(CH_3CN)_4]PF_6$ (0.495 g, 1.33 mmol) and PCy_3 (0.750 g, 2.68 mmol) in acetone (15 mL) was stirred at room temperature for 3 h. After filtration, the solvent was removed and the resultant white solid was washed with diethyl ether. A white crystalline solid was obtained upon recrystallization of the crude solid in CH_2Cl_2/diethyl ether (0.652 mg, 64%). $^{31}P[^1H]$ NMR (202 MHz, $CDCl_3$, 298 K): $\delta = 24.6$ ppm; MS(FAB): m/z: 624 $[M^+ - PF_6]$; elemental analyses calcd (%) for $C_{36}H_{66}P_3F_6Cu$ (769.34): C 56.20, H 8.65; found: C 55.92, H 8.48.

$[Cu(dcpm)_2]PF_6$ (8): A mixture of $[Cu(CH_3CN)_4]PF_6$ (0.038 g, 0.1 mmol) and dcpm (0.096 g, 0.2 mmol) in dichloromethane (10 mL) was stirred for 12 h. Upon removal of solvent and addition of diethyl ether, a white solid was obtained, which was recrystallized by diffusing diethyl ether into the dichloromethane solution (0.086 g, 84%). $^{31}P[^1H]$ NMR (202 MHz, $CDCl_3$, 298 K): $\delta = 13.7$ ppm; IR (Nujol): $\tilde{\nu} = 831$ cm^{-1} (PF_6^-); MS(FAB): m/z 880 $[M^+ - PF_6]$; elemental analyses calcd (%) for $C_{50}H_{92}P_5F_6Cu$ (1025.63): C 58.55, H 9.04; found: C 58.33, H 9.15.

$[Cu_2(dmpm)_3](ClO_4)_2$ (9): $[Cu(CH_3CN)_4]ClO_4$ (0.327 g, 1 mmol) was suspended in acetone (20 mL), and dmpm (0.274 g, 2 mmol) was added until a colorless solution was obtained. After stirring for 12 h, the volume of the reaction mixture was reduced to about 5 mL. Precipitation was induced by addition of diethyl ether. The crude product was recrystallized in acetone/diethyl ether (0.294 g, 80%). $^{31}P[^1H]$ NMR (202 MHz, $[D_6]$acetone, 298 K): $\delta = -27.5$ ppm; IR (Nujol): $\tilde{\nu} = 1098$ cm^{-1} (br, ClO_4^-); MS(FAB): m/z:635 $[M^+ - ClO_4]$; elemental analyses calcd (%) for $C_{15}H_{42}P_6Cu_2Cl_2O_8$ (734.33): C 24.53, H 5.76; found: C 24.31, H 5.90.

Instrumentation and physical measurements: ^{31}P (202 MHz) NMR spectra were recorded on Bruker DPX-500 multinuclear FT-NMR spectrometers. Chemical shifts (δ, ppm) are reported relative to 85% H_3PO_4. IR spectra were obtained on a Bio-Rad FTS-165 spectrometer. UV-visible spectra were obtained on a Hewlett-Packard 8453 diode array spectrometer. Positive ion FAB mass spectra were recorded on a Finnigan MAT 95 mass spectrometer with 3-nitrobenzyl alcohol (NBA) as a matrix. Elemental analysis was performed on a Carlo Erba 1106 elemental analyzer at the Institute of Chemistry, Chinese Academy of Sciences. Emission and excitation were obtained on a SPEX 1681 Fluorolog-2 Model F111AI fluorescence spectrophotometer equipped with a Hamamatsu R928 PMT detector. For solution emission and excitation spectra, samples were degassed on a high vacuum line. The solutions were subjected to at least four freeze-pump-thaw cycles. Emission lifetime measurements were performed with Quanta Ray DCR-3 pulsed Nd:YAG laser system (pulse output 266 or 355 nm, 8 ns). The emission signals were detected by a Hamamatsu R928 photomultiplier tube and recorded on a Tektronix model 2430 digital oscilloscope. The emission quantum yields of solutions were measured by the method of Demas and Crosby[28] with quinine sulfate in degassed 0.1N sulfuric acid as the standard ($\Phi_r = 0.546$) and calculated by $\Phi_s = \Phi_r(B_r/B_s)(n_s/n_r)^2(D_s/D_r)$, in which the subscripts s and r refer to sample and reference standard solution respectively, n is the refractive index of the solvents, D is the integrated intensity, and Φ is the luminescence quantum yield. The quantity B is calculated by $B = 1 - 10^{-AL}$, in which A is the absorbance at the excitation wavelength and L is the optical path length. Emission quenching was performed by lifetime measurements, and the quenching rate constant, k_q, was deduced from the plot of $1/t$ versus [Q] according to the Stern–Volmer equation $\tau_0/\tau = 1 + k_q\tau_0[Q]$, in which τ_0 and

τ are the respective emission lifetimes in the absence and presence of quencher Q.

Transient absorption difference spectra were recorded after excitation of the sample in degassed solution with a 8 ns laser pulse at $\lambda = 355$ nm. The monitoring beam was provided by a 300 W continuous-wave xenon lamp that was oriented perpendicular to the direction of the laser pulse. The transient absorption signals at each wavelength were collected with a SpectraPro-275 monochromator operating with 2 mm slits, with the signal fed to a Tektronix TDS 520D oscilloscope. The optical difference spectrum was generated point-by-point by monitoring at individual wavelengths.

CCDC-142369 (**1**), CCDC-142370 (**2**), CCDC-142371 (**3**), CCDC-142609 (**4**), CCDC-142372 (**5**), CCDC-142373 (**6**), CCDC-195956 (**7**), CCDC-195955 (**8**), and CCDC-195957 (**9**) contain the supplementary crystallographic data for this paper. These data can be obtained free of charge via www.ccdc.cam.ac.uk/conts/retrieving.html (or from the Cambridge Crystallographic Data Centre, 12 Union Road, Cambridge CB21EZ, UK; fax: (+44) 1223-336-033; or e-mail: deposit@ccdc.cam.ac.uk).

Acknowledgement

We are grateful for financial support from the Research Grants Council of the Hong Kong SAR, China [HKU 7298/99P], the Large Equipment Funding Scheme of the University of Hong Kong, and The Croucher Foundation (Hong Kong).

[1] a) C. Kutal, *Coord. Chem. Rev.* **1990**, *99*, 213 – 252; b) P. C. Ford, A. Vogler, *Acc. Chem. Res.* **1993**, *26*, 220 – 226; c) O. Horváth, *Coord. Chem. Rev.* **1994**, *135/136*, 303 – 324; d) D. R. McMillin, K. M. McNett, *Chem. Rev.* **1998**, *98*, 1201 – 1219; e) P. C. Ford, E. Cariati, J. Bourassa, *Chem. Rev.* **1999**, *99*, 3625 – 3647.

[2] E. Cariati, J. Bourassa, P. C. Ford, *Chem. Commun*. **1998**, 1623 – 1624.

[3] Y.-G. Ma, W.-H Chan, X.-M. Zhou, C.-M. Che, *New J. Chem*. **1999**, 263 – 265.

[4] a) D. V. Scaltrito, D. W. Thompson, J. A. O'Callaghan, G. J. Meyer, *Coord. Chem. Rev.* **2000**, *208*, 243 – 266; b) N. Armaroli, *Chem. Soc. Rev.* **2001**, *30*, 113 – 124.

[5] a) F. Sabin, C. K. Ryu, P. C. Ford, A. Vogler, *Inorg. Chem*. **1992**, *31*, 1941 – 1945; b) C.-K. Chan, C.-X. Guo, R.-J. Wang, T. C. W. Mak, C.-M. Che, *J. Chem. Soc. Dalton Trans.* **1995**, 753 – 757; c) C.-K. Chan, K.-K. Cheung, C.-M. Che, *Chem. Commun*. **1996**, 227 – 228; d) V. W.-W. Yam, K. K.-W. Lo, *Comments Inorg. Chem*. **1997**, *19*, 209 – 229.

[6] a) J. D. Barrie, B. Dunn, G. Hollingsworth, J. I. Zink, *J. Phy. Chem*. **1989**, *93*, 3958 – 3963; b) R. Provencher, P. D. Harvey, *Inorg. Chem*. **1996**, *35*, 2235 – 2241; c) P. D. Harvey, M. Drouin, T. Zhang, *Inorg. Chem*. **1997**, *36*, 4998 – 5005; d) V. W.-W. Yam, K. K.-W. Lo, W. K.-M. Fung, C.-R. Wang, *Coord. Chem. Rev.* **1998**, *171*, 17 – 41.

[7] C.-M. Che, Z. Mao, V. M. Miskowski, M.-C. Tse, C.-K. Chan, K.-K. Cheung, D. L. Phillips, K.-H. Leung, *Angew. Chem.* **2000**, *112*, 4250 – 4254; *Angew. Chem. Int. Ed*. **2000**, *39*, 4084 – 4088.

[8] a) C.-M. Che, H.-L. Kwong, C.-K. Poon, V. W.-W. Yam, *J. Chem. Soc. Dalton Trans.* **1990**, 3215 – 3219; b) V. W.-W. Yam, T.-F. Lai, C.-M. Che, *J. Chem. Soc. Dalton Trans.* **1990**, 3747 – 3752; c) T. M. McCleskey, H. B. Gray, *Inorg. Chem*. **1992**, *31*, 1733 – 1734; d) W.-H. Chan, T. C. W. Mak, C.-M. Che, *J. Chem. Soc. Dalton Trans.* **1998**, 2275 – 2276; e) W.-F. Fu, K.-C. Chan, K.-K. Cheung, C.-M. Che, *Chem. Eur. J.* **2001**, *7*, 4656 – 4664.

[9] a) P. D. Akrivos, P. P. Karagiannidis, C. P. Raptopoulou, A. Terzis, S. Stoyanov, *Inorg. Chem*. **1996**, *35*, 4082 – 4083; b) E. W. Ainscough, A. M. Brodie, A. K. Burrell, J. V. Hanna, P. C. Healy, J. M. Waters, *Inorg. Chem*. **1999**, *38*, 201 – 203.

[10] B. F. Straub, F. Rominger, P. Hofmann, *Inorg. Chem*. **2000**, *39*, 2113 – 2119.

[11] F. G. Moers, P. H. Ophetveld, *J. Inorg. Nucl. Chem*. **1970**, *22*, 3225 – 3228.

[12] M. Doyle, W. Parker, P. A. Gunn, J. Martin, D. D. Macnicol, *Tetrahedron Lett*. **1970**, *42*, 3619 – 3622.

[13] L. Manojlović-Muir, K. W. Muir, *J. Chem. Soc. Chem. Commun*. **1982**, 1155 – 1156.

[14] W. Bensch, M. Prelati, W. Ludwig, *J. Chem. Soc. Chem. Commun*. **1986**, 1762 – 1763.

[15] R. J. Restivo, A. Costin, G. Ferguson, A. J. Carty, *Can. J. Chem*. **1975**, *53*, 1949 – 1957.

[16] Because **1** is only sparingly soluble in MeOH, a mixed solvent system of CH_2Cl_2/MeOH (1:1) was used.

[17] D. Li, C.-M. Che, W.-T. Wong, S.-J. Shieh, S.-M. Peng, *J. Chem. Soc. Dalton Trans.* **1993**, 653 – 654.

[18] W.-F. Fu, K.-C. Chan, V. M. Miskowski, C.-M. Che, *Angew. Chem.* **1999**, *111*, 2953 – 2955; *Angew. Chem. Int. Ed.* **1999**, *38*, 2783 – 2785.

[19] M. R. Churchill, F. J. Rotella, *Inorg. Chem*. **1979**, *18*, 166 – 171.

[20] G. L. Soloveichik, O. Eisenstein, J. T. Poulton, W. E. Streib, J. C. Huffman, K. G. Caulton, *Inorg. Chem*. **1992**, *31*, 3306 – 3312.

[21] We cannot test for cases where $n > 3$ because the number of experimental data needed for the fitting is very large. We propose that the number of CH_3CN molecules (n) reacting with the $[Cu_2(dcpm)_2]^{2+}$ moiety is not less than three (see Supporting Information for details).

[22] J. Díez, M. P. Gamasa, J. Gimeno, A. Tiripicchio, M. T. Camellini, *J. Chem. Soc. Dalton Trans.* **1987**, 1275 – 1278.

[23] K. H. Leung, D. L. Phillips, Z. Mao, C.-M. Che, V. M. Miskowski, C.-K. Chan, *Inorg. Chem*. **2002**, *41*, 2054 – 2059.

[24] D. Li, C.-M. Che, H.-L. Kwong, V. W.-W. Yam, *J. Chem. Soc. Dalton Trans*. **1992**, 3325 – 3329.

[25] M. Sakamoto, A. Ueno, H. Mihara, *Chem. Eur. J.* **2001**, *7*, 2449 – 2458.

[26] G. J. Kubas, *Inorg. Synth.* **1979**, *19*, 90 – 92.

[27] S.-W. Lai, M. C.-W. Chan, T.-C. Cheung, S.-M. Peng, C.-M. Che, *Inorg. Chem.* **1999**, *38*, 4046 – 4055.

[28] J. N. Demas, G. A. Crosby, *J. Phys. Chem.* **1971**, *75*, 991 – 1024.

Received: November 25, 2002 [F4610]

2armige Pfeile

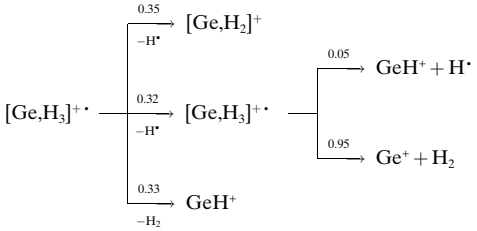

(2)

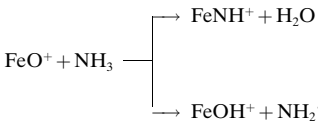

(5a)

(5b)

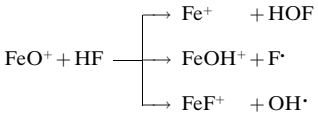

(7a)

(7b)

(7c)

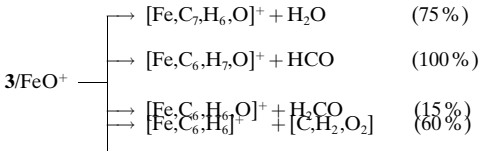

(5a)

(5b)

(5c)

(5d)

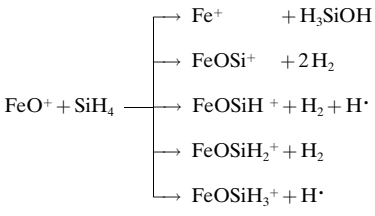

(9a)

(9b)

(9c)

(9d)

(9e)

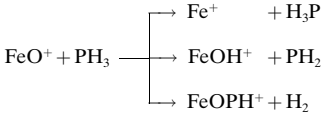

(12a)

(12b)

(12c)

3armige Pfeile und rechts

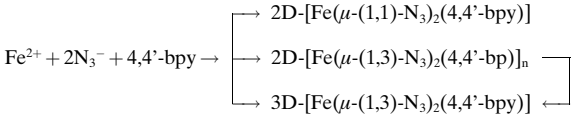

\def\bindous{\limits _{\scale 160% \mid}^{\smash {\vskip -0.25em {\scale 160% \mid}}}}

\def\bindos{\limits _{\phantom \mid}^{\smash {\vskip -0.25em {\scale 160% \mid}}}}

\def\bindus{\limits _{\scale 160% \mid}^{\smash {\vskip -0.25em {\phantom \mid}}}}

Thr

$$G(t) = 1 + \frac{1}{\mathrm{N}}\left(\frac{1}{1 + \frac{4Dt}{r^2}}\right) \tag{1}$$

Pfeil mit x

$$\mathbf{a} + \mathrm{Cl_2} \nrightarrow \mathbf{b} + \mathrm{HCl} \tag{3}$$

Buchstabe mit Übersetzer-Pfeil

$\vec{k}$

$\vec{k}$

'Umkehrpfeil oben groß unten klein, rechts

$\rightleftharpoons$

'Umkehrpfeil oben groß unten klein, links

$\rightleftharpoons$

'Spezialformeln aus Beitrag F01688

$$k_{\mathrm{ET}} = \sqrt{\frac{\pi}{\hbar^2 \lambda_s k_b T}}\,|V|^2 \sum_{n}^{\infty}(e^{-S}S^n/n!)\exp\left(-\frac{(\lambda_s + \Delta G + n\hbar\langle\omega\rangle)^2}{4\lambda_s k_b T}\right) \tag{10}$$

'Spezialformeln aus Beitrag F01732

$$\begin{aligned} Q_{\mathrm{A}}^{\mathrm{VDD}} &= Q_{\mathrm{A,pair}}^{\mathrm{VDD}} - Q_{\mathrm{A,base}}^{\mathrm{VDD}} \\ &= -\left[\int\limits_{\substack{\text{Voronoi cell}\\ \text{of A in pair}}} (\rho_{\mathrm{pair}}(\mathbf{r}) - \Sigma_{\mathrm{B}}\rho_{\mathrm{B}}(\mathbf{r}))d\mathbf{r}\right. \\ &\quad \left. - \int\limits_{\substack{\text{Voronoi cell}\\ \text{of A in base}}} (\rho_{\mathrm{base}}(\mathbf{r}) - \Sigma_{\mathrm{B}}\rho_{\mathrm{B}}(\mathbf{r}))d\mathbf{r}\right] \end{aligned} \tag{6}$$

$$\Delta Q_{\mathrm{A}}^{\Gamma} = -\int\limits_{\substack{\text{Voronoi cell}\\ \text{of A in pair}}} [\rho_{\mathrm{pair}}^{\Gamma}(\mathbf{r}) - \rho_{\mathrm{base1}}^{\varrho}(\mathbf{r}) - {}^{\Gamma}_{\mathrm{base2}}(\mathbf{r})]d\mathbf{r} \tag{8}$$

$$\rho^{\Gamma} = \sum_{i\in\Gamma}^{occ} |\psi_i^{\Gamma}|^2 \tag{9}$$

Table 3. Electrochemical data for ferrocenylimines.[a]

Half reaction	E_{pa}[b] [V]	E_{pc}[c] [V]	$E_{1/2}$[d] [V]	$\frac{n_{app}}{[Fe]_T}$[e]
$[Fe^{II}]$ (**5**) $\rightleftharpoons [Fe^{III}]^+$ (**5**$^+$)+e$^-$	0.64	0.54	0.59 (0.1)	1
$[(Fe^{II})_2]$ (**6**) $\rightleftharpoons$ $[Fe^{II}Fe^{III}]^+$ (**6**$^+$)+e$^-$	0.57	0.50	0.54 (0.07)	0.5
$[Fe^{II}Fe^{III}]^+$ (**6**$^+$) $\rightarrow [(Fe^{III})_2]^{2+}$ (**6**$^{2+}$)+e$^-$	0.70	0.64	0.67 (0.06)	0.5

[a] Solvent = CH_3CN, supporting electrolyte = 0.1 mol L^{-1} $TBABF_4$. [b] Oxidation peak potential in V vs. Ag/AgCl determined by cyclic voltammetry. Sweep rate = 100 mV s^{-1}. Ferrocene/ferrocenium redox couple was 0.40 V vs. this Ag/AgCl. [c] Reduction peak potential. [d] (E_{pa}+E_{pc})/2. ΔE_p (= $E_{pa} - E_{pc}$, at 100 mV s^{-1}) given in parenthesis. [e] Number of electrons per mole of iron.

'Linien in Tabellen

